RSC Advances

PAPER

View Article Online
View Journal | View Issue

Cite this: *RSC Adv.*, 2025, **15**, 19023

Redispersible CuO nanoparticles: preparation and photocatalytic capacity for the degradation of methylene blue†

Qianwen Wang, Guanbin Gao, Depeng Gong and Chaocan Zhang *

In this study, redispersible copper oxide nanoparticles (CuO NPs) with an average size of 92.18 nm were synthesized using ethylene glycol as a complexing agent and sodium poly(4-styrenesulfonic acid-*co*-maleic acid) as a stabilizer. The CuO NP dispersion remained stable for 30 days. In the CuO NPs/methylene blue (MB) system, the MB absorption peak at 664 nm weakened or disappeared, while a new peak at 583 nm emerged, indicating the formation of a charge-interaction complex confirmed by zeta potential measurements. Under UV irradiation, CuO NPs showed weak photocatalytic activity, degrading MB by 8.7%, 8.8%, and 9.7% at dosages of 1.3, 1.9, and 2.5 mM, respectively. At 0.6 mM CuO NPs, flocculation occurred, and FT-IR analysis confirmed MB adsorption onto CuO NPs with a capacity of 217.4 mg g^{-1}, indicating that MB was mainly separated from the system through adsorption by CuO NPs rather than being degraded *via* photocatalysis. With hydrogen peroxide, CuO NPs achieved nearly complete photodegradation (99.6%) of 53.5 μM MB within 75 minutes. This work offers novel insights into the development of redispersible nanomaterials and their applications in water treatment.

Received 31st March 2025
Accepted 30th May 2025

DOI: 10.1039/d5ra02244d

rsc.li/rsc-advances

1 Introduction

With the rapid development of industries such as textiles, papermaking, pharmaceuticals, and cosmetics, approximately several million tons of dye-containing wastewater are discharged into rivers and lakes every year, and the discharges contain numerous colored organic compounds, which have become one of the major sources of water resource pollution.[1] Organic dyes such as methylene blue (MB) account for a large proportion of the emissions. MB is a blue-green cationic dye[2] belonging to the phenothiazine family,[3] and is water-soluble and toxic.[4,5] When the human body is exposed to MB, it may give rise to adverse reactions such as nausea, vomiting, and dyspnea. Meanwhile, it can also irritate the oral cavity, throat, esophagus, and stomach, leading to a series of symptoms including abdominal discomfort and diarrhea.[6] Efficiently treating and degrading dyes such as MB in water has become an urgent issue that needs to be addressed. Currently, photocatalysis is a highly effective approach to dealing with water pollution problems. Photocatalysis[7–9] can not only achieve the decolorization of pollutants but also completely mineralize them,[7] converting them into simple small molecular substances, thus achieving the goal of eliminating pollutants. In the field of photocatalysis, nano-copper oxide (nano-CuO) has received extensive attention and has become one of the candidate materials with great development potential.

Copper oxide is a p-type narrow bandgap semiconductor material. The bandgap of the bulk form ranges from 1.2 to 1.7 electronvolts (eV),[10] and it exhibits excellent absorbance in the ultraviolet-visible light region and a relatively broad luminescence intensity.[11] Nano-CuO has the adaptability to different length scales and diverse morphological characteristics, including nanowires, nanoflowers, nanorods, nanospheres,[12–15] *etc.* Moreover, it is of low cost, not as expensive as precious metals such as gold, silver, and platinum. Additionally, it possesses high physical and chemical stability, and thus exhibits application values in numerous fields, such as biomedicine,[16] optoelectronics,[17] environmental remediation,[18] electrochemistry,[19] photocatalysis,[10] energy storage and conversion,[20] solar cells, and sensing.[21,22] For instance, the research by Raizada *et al.*[23] has shown that copper oxide nanoparticles exhibit attractive physical and chemical properties, including a large specific surface area, appropriate redox potential, excellent electrochemical activity, and ultra – high thermal conductivity.

The preparation technology of nano-CuO has always been the focus of attention in the scientific research and industrial communities. Numerous scholars have successively reported various preparation methods for nano-copper oxide particles, including the precipitation method,[24] sol–gel method,[25] hydrothermal method,[26] microemulsion method,[27] and wet chemistry method.[28,29] Muthuvel *et al.*[30] used copper nitrate as the copper source and synthesized spherical nano-copper oxide through

School of Materials Science and Engineering, Wuhan University of Technology, Wuhan 430070, China. E-mail: polymers@whut.edu.cn

† Electronic supplementary information (ESI) available. See DOI: https://doi.org/10.1039/d5ra02244d

the sol–gel method. According to the analysis by transmission electron microscopy, the average diameter of the microspheres in the aggregates was 32 nm. Under exposure to sunlight, its degradation efficiency for MB reached 85%. Anna *et al.*[31] used copper chloride dihydrate as the copper source, cetyltrimethylammonium bromide as the surfactant, and sodium borohydride as the reducing agent. They prepared cubic nano-copper oxide with a size of 52 ± 2 nm through a chemical reduction method and discussed its photocatalytic activity. Under natural light, the degradation efficiency of the nano-copper oxide for MB reached 84% within 240 minutes. Benhadria *et al.*[32] used copper sulfate as the copper source, and sodium dodecyl sulfate and cetyltrimethylammonium bromide as surfactants, and synthesized copper oxide nanoparticles by the precipitation method. These particles were composed of granular sheets with a diameter of 100–200 nm. In the catalytic degradation of MB, the products prepared with sodium dodecyl sulfate completely degraded MB within 10 minutes. Rakshit *et al.*[33] successfully prepared copper oxide nanorods (CuO NRs) using different precursors through a one-step chemical method. Field emission transmission electron microscopy analysis confirmed the presence of highly crystalline CuO NRs, with an average length of 100–500 nm and a diameter of 20–150 nm. When studying the photocatalytic performance of CuO NRs on MB under visible light, it was found that when only CuO NRs were used, the adsorption amount of MB dye pollutants was very small. However, when hydrogen peroxide was present simultaneously, CuO NRs exhibited enhanced catalytic activity for the degradation of MB, with a degradation efficiency of more than 80% within 60 minutes. Neto *et al.*[34] prepared nano-copper oxide for the photocatalysis of MB through the sonochemical method. Using copper nitrate as the copper source, they employed different surfactants (cetyltrimethylammonium bromide, ethylenediamine, polyethylene glycol). The prepared products all exhibited good photocatalytic activity. Shaheen and his team[35] used copper sulfate as the raw material and synthesized pure nano-copper oxide as well as nano-copper oxide stabilized by Triton X-100 and cetyl alcohol respectively through the precipitation method. These were then applied to the degradation of MB dye under sunlight. The results showed that, within the same time period, the degradation rate of MB by pure nano-copper oxide reached 85.5% within 300 minutes, while those by the surfactants-modified nano-copper oxide reached 80.8% and 75.8% respectively. However, during the preparation and analysis of most copper oxide nanoparticles, due to the intermolecular van der Waals forces existing on the surface area per unit volume of the material, there is a strong attractive force between the particles, which makes the particles prone to agglomeration.[36] This agglomeration phenomenon may have a negative impact on the performance of copper oxide nanoparticles in practical applications. For example, in photocatalysis, the aggregation of small-sized particles into larger ones not only reduces the effective volume fraction of the material and decreases the number of photocatalytic active sites, but also affects the stability of the catalyst and the durability of the catalytic process.[37,38] For nanomaterials, redispersibility is not only a crucial factor for maintaining their structural integrity but also an inherent requirement for preserving their intrinsic physical and chemical properties. At present, relevant reports on the direct preparation of redispersible nano-CuO are still scarce.

Our research group previously reported a method for preparing magnetic-responsive photonic crystals of nano-Fe_3O_4.[39] The nano-Fe_3O_4 prepared by this method has excellent monodispersity and uniform particle size, which can provide a good idea for the preparation of redispersible copper oxide nanoparticles. Based on this, in this study, ethylene glycol was used as a complexing agent and sodium poly(4-styrenesulfonic acid-*co*-maleic acid) as a protective agent to further explore the efficient preparation of redispersible copper oxide nanoparticles. After the preparation was completed, the size, crystal structure, surface properties and other aspects of the obtained products were characterized, and its stability when redispersed in water was investigated. Eventually, the prepared copper oxide nanoparticles were employed as photocatalysts in the catalytic degradation study of the harmful organic dye MB. The results showed that the photocatalytic ability of the copper oxide nanoparticles stably dispersed in the solution was very weak. In contrast, the flocculated and precipitated nanoscale copper oxide adsorbed and removed MB from the solution in the form of charge complexes, indicating that its direct photocatalytic ability was relatively weak. However, with the enhanced assistance of hydrogen peroxide, the copper oxide nanoparticles exhibited excellent photocatalytic performance.

2 Material and experimental

2.1 Materials

Copper chloride dihydrate ($CuCl_2 \cdot 2H_2O$, CAS: 10125-13-0) and polyvinylpyrrolidone (PVP, $M_w \approx 24\,000$, CAS: 9003-39-8) were purchased from Shanghai Macklin Biochemical Co., Ltd; sodium poly(4-styrenesulfonic acid-*co*-maleic acid) (PSSMA, $M_w \approx 20\,000$, SS : MA = 1 : 1, CAS: 68037-40-1) and methylene blue trihydrate ($C_{16}H_{18}ClN_3S \cdot 3H_2O$, CAS: 7220-79-3) were both purchased from Shanghai Aladdin Biochemical Technology Co., Ltd; sodium hydroxide (NaOH), cetyltrimethylammonium bromide (CTAB), and ethylene glycol (EG) were purchased from Sinopharm Chemical Reagent Co., Ltd; hydrogen peroxide (H_2O_2, 30%) was purchased from Binqi (Shanghai) Environmental Technology Co., Ltd; deionized water was self-prepared in the laboratory; acetone was purchased from Shiyou Chemical (Yangzhou) Co., Ltd. All of the above chemicals were of analytical grade purity, did not require further purification, and were stored according to the storage conditions.

2.2 Preparation of copper oxide nanoparticles

First, 10 mL of EG, 0.34 g of $CuCl_2 \cdot 2H_2O$, and 0.15 g of PSSMA were weighed out and added sequentially to a beaker containing 20 mL of deionized water. The mixture was stirred until complete dissolution, yielding a sky-blue solution. Subsequently, the beaker was transferred to an intelligent magnetic heating stirrer and gradually heated to 100 °C under stirring. Then, 0.16 g of NaOH was rapidly added to the mixed solution,

followed by continuous stirring for 20 minutes. The mixed solution gradually changed in color from sky blue to blue-green and then to black. After the reaction was completed, the obtained solution was allowed to cool naturally at room temperature. The preparation procedure with CTAB and PVP addition followed the same protocol as that of PSSMA. Then, the solution was transferred into a centrifuge tube and placed in a centrifuge. It was centrifuged at a speed of 8000 rpm to collect the black product, which was then washed multiple times with a mixed solution of deionized water and acetone. Finally, the copper oxide nanoparticles were dried and stored for subsequent characterization.

2.3 Material characterization

The crystal form of the collected products was characterized by an Empyrean X-ray diffractometer manufactured by PANalytical B.V., Netherlands. The XRD spectrum was measured within the range of $2\theta = 20°$ to 80°, and was compared with the PDF cards of the International Centre for Diffraction Data (ICDD). The morphology of the samples was characterized by a JEM-F200 field emission transmission electron microscope manufactured by JEOL Ltd, Japan. The oxidation state of copper in the synthesized products was characterized by a Thermo Scientific ESCALAB 250Xi X-ray photoelectron spectrometer manufactured by Thermo Fisher Scientific Inc., USA. The groups of the samples were determined using a microscopic Fourier transform infrared spectroscopy system (400–4000 cm^{-1}) from Thermo Fisher Scientific iN10-iS50, USA. The potential and particle size of the products were tested using a Malvern Zetasizer Nano ZS90 nanoparticle size and zeta potential analyzer (DLS) (UK) and the samples were prepared by ultrasonication dispersed in deionized water. The products were optically characterized using a UV-9000s UV-visible spectrophotometer from Shanghai Yuan Analytical Instrument Co. Ltd, China, and the spectra were recorded in the UV-visible range (200–800 nm) with a scanning interval of 1.0 nm.

2.4 Evaluation of redispersible properties of copper oxide nanoparticles

The copper oxide nanoparticles (CuO NPs) dispersion was prepared by redispersing the CuO NPs powder in deionized water at room temperature. To accurately characterize its dispersion stability, the following two methods were adopted in this study: (1) the static settlement method. The dispersion was placed in a glass bottle and subjected to a long-term static settlement treatment. Subsequently, the sedimentation situation was carefully observed by taking photos. Based on this, the stability of the dispersion could be evaluated intuitively and effectively. This method is relatively simple to operate and can reflect the stability changes of the nanofluid under the action of gravity from a macroscopic perspective. (2) The zeta potential method. The zeta potential is an important parameter for characterizing the stability of a colloidal dispersion system, which reflects the equilibrium relationship between the electrostatic repulsive force generated by the charges on the particle surface and the van der Waals attractive force. In this study, the numerical range around +30 mV or −30 mV was used as the basis for judging the dispersion stability of the nanoparticles.[40]

2.5 Exploration of the photocatalytic capability of copper oxide nanoparticles

In this study, methylene blue was used as the target pollutant. Appropriate amounts of methylene blue solutions with different concentrations were taken into cuvettes. Using deionized water as the blank control group, the absorbance of the solutions at a wavelength of 664 nm was measured with an ultraviolet-visible spectrophotometer. With the concentration c as the abscissa and the corresponding absorbance A as the ordinate, the obtained data were linearly fitted. Finally, the standard curve equation correlating the concentration of methylene blue solution with absorbance is presented in ESI Fig. S1.† During the photocatalytic degradation process, a 6 w ultraviolet (UV) light source with a wavelength of 365 nm was used as the irradiation source, operating at 25 °C with the light source maintained at a distance of 15 cm from the sample. 40 mL of methylene blue aqueous solution with a concentration of 53.5 μM was taken and placed in a quartz reagent bottle, and 0.6 mM of CuO NPs powder catalyst was added thereto to form a photocatalytic reaction system. In addition, hydrogen peroxide was added to the above reaction solution as an electron sacrificial agent. The adsorption capacity and degradation rate of methylene blue were calculated by eqn (1) and (2) respectively:

$$q_m = \frac{(c_0 - c_t)}{m} V \quad (1)$$

$$\text{degradation rate}(\%) = \left(\frac{c_0 - c_t}{c_0}\right) \times 100\% \quad (2)$$

where c_0 is the initial concentration of the dye, c_t is the concentration of the dye at time t, V is the volume of the solution (L), m is the mass of the CuO NPs (g), and q_m is the adsorption capacity (mg g^{-1}).

3 Results and discussion

3.1 Preparation and structural characterization of redispersible copper oxide nanoparticles (CuO NPs)

When preparing redispersible CuO NPs, copper chloride dihydrate ($CuCl_2 \cdot 2H_2O$) was used as the copper source. A mixed solvent composed of ethylene glycol (EG) as the complexing agent and deionized water (DI) was employed. $CuCl_2 \cdot 2H_2O$ was dissolved in this mixed solvent, and sodium poly(4-styrenesulfonic acid-*co*-maleic acid) (PSSMA), cetyltrimethylammonium bromide (CTAB), and polyvinylpyrrolidone (PVP) (see ESI, Tables S1, S2 and Fig. S2†) were separately added as a protective agent to assist in the formation of redispersible CuO NPs. A batch of products was synthesized by adjusting the addition amounts of EG, PSSMA, CTAB and PVP. The experimental results are shown in Tables 1, ESI, S1 and S2,† respectively. When neither EG nor PSSMA was added to the system, the average particle size of the prepared products was relatively large, reaching 337.07 nm (Sample No. 1). When a certain amount of EG was added to the system, the particle

Table 1 Preparation of products with different EG and PSSMA dosages

	Precursors	Products			
Sample no	DI (mL)	EG (mL)	PSSMA (g)	Average size (nm)	PDI
1	20	0	0	337.07	0.379
2	20	5	0	239.07	0.329
3	20	10	0	216	0.308
4	20	15	0	246.08	0.35
5	20	20	0	279.36	0.425
6	20	10	0.15	92.18	0.294
7	20	10	0.30	115	0.216
8	20	10	0.45	115.19	0.41
9	20	10	0.60	119.49	0.46
10	20	10	0.75	122.5	0.449

size of the prepared products significantly decreased, and the dispersibility was improved (Samples No. 2–5). When 0.15 g PSSMA was added to the system, the average particle size of the synthesized product decreased to 92.18 nm. However, when a relatively large amount of PSSMA was added to the system, the PDI index of the products suddenly increased. This might be because the adsorption of PSSMA on the surface of the products was uneven, resulting in different growth rates of the products in various directions. Consequently, the particle size distribution became inhomogeneous, and the PDI index rose.

In order to study the crystal structure of the synthesized products, the Sample No. 6 was characterized by X-ray diffraction (XRD) tests at different experimental parameters (all subsequent studies were conducted using Sample No. 6). The crystal structure of the prepared copper oxide nanoparticles was analyzed by powder X-ray diffraction technique within the range of 2θ = 20–80°. The results are shown in Fig. 1(b). A series of diffraction peaks appear at 2θ values of 32.2°, 35.4°, 38.3°, 49.3°, 52.5°, 57.9°, 61.6°, 66.4°, 68.3° and 75.0°. After a careful comparison with the data of the copper oxide PDF #89-2531 standard card, these diffraction peaks correspond to the (110), (−111), (111), (−202), (020), (202), (−113), (−311), (−221) and (004) crystal planes in sequence. In the entire diffraction pattern, no diffraction peaks of impurities are observed, and it is in high agreement with the data on the card. This confirms the formation of the pure-phase copper oxide with a monoclinic structure. The XRD patterns are indexed in the monoclinic system with the lattice parameters of $a = 4.7915$ Å, $b = 3.4328$ Å, $c = 5.1626$ Å, and $\beta = 101.21°$. Subsequently, the crystallite size, unit cell volume, and crystallinity were calculated using the following equations:

$$D = \frac{0.9\lambda}{\beta \cos \theta} \quad (3)$$

where D is the crystallite size, β is the full width half maxima (FWHM) in radians and θ is the diffraction angle in degrees.

$$V = abc \sin \beta \quad (4)$$

$$X_c = \frac{A_c}{A_c + A_{am}} \times 100\% \quad (5)$$

where V is the volume of unit cell, β is the included angle between a and c; X_c denotes the crystallinity, A_c represents the total area of crystalline peaks, and A_{am} refers to the area of amorphous scattering. The crystallite size of copper oxide was determined to be 4.8 nm using the Scherrer equation (eqn (3)), with a corresponding unit cell volume of 83.2 Å^3 and a crystallinity of 44.13%. In fact, the initial indication of the formation of copper oxide nanoparticles can be intuitively determined by the color change of the solution from blue to brown-black. As shown in Fig. 1(a), this color change is attributed to the surface plasmon resonance generated during the formation of nano-copper oxide. This phenomenon causes the absorption and scattering characteristics of the nanoparticles to specific wavelengths of light to change.[41]

The hydrodynamic diameter was characterized by intensity-, number-, and volume-weighted distributions, as shown in Fig. 2(a–c), with corresponding values of 83.20, 35.31, and 49.12 nm, respectively. Notably, the number-weighted size

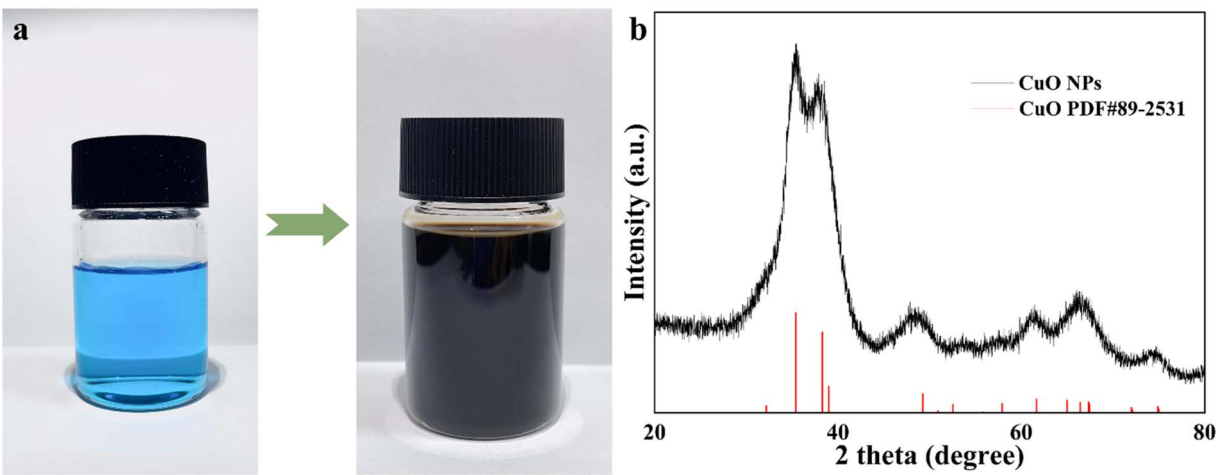

Fig. 1 (a) Optical photographs of the color change of the solution before and after the reaction (precursor on the left side, product on the right side); (b) XRD pattern of Sample No. 6.

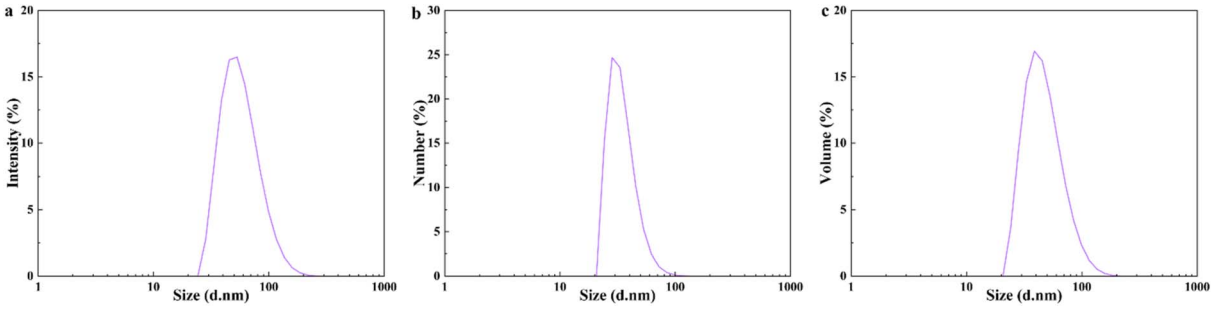

Fig. 2 The particle size of Sample No. 6 (a) intensity-based; (b) number-based; (c) volume-based size distribution.

distribution exhibited smaller particle dimensions with the highest intensity, which is consistent with the findings reported by Bin Mobarak *et al.*[42]

The light absorption characteristics of the prepared nano-copper oxide (Sample No. 6) were characterized by ultraviolet-visible light spectroscopy. The result shows that it exhibits strong absorbance and a broad absorption peak within the ultraviolet-visible light range. The maximum absorption peak appears at 373 nm, as shown in Fig. 3(a). This result is consistent with the maximum absorbance reported by Kasana *et al.*[43] in the literature. The emergence of the absorption peak at 373 nm is attributed to the surface plasmon absorption phenomenon of the metal oxide, indicating the formation of nano-copper oxide particles. This is caused by the interband transition of the core electrons of the nano-copper oxide.

The Tauc plot method was used to determine the optical direct bandgap energy of the allowed optical transitions of copper oxide nanoparticles, and the relationship is expressed as:

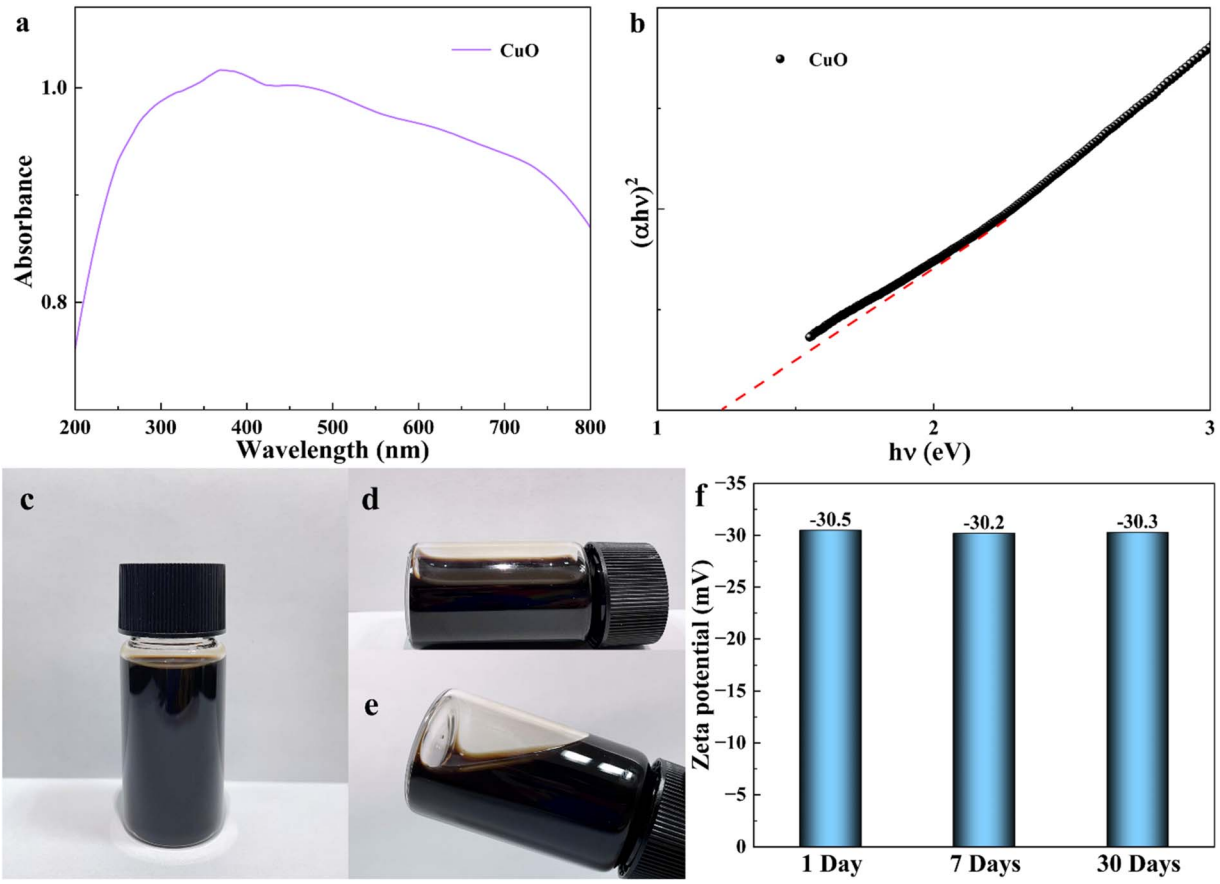

Fig. 3 (a) UV-vis spectrum of nano-CuO; (b) Tauc plot of the direct structural transformation of nano-CuO; (c) optical photograph of nano-CuO after standing for 1 day; (d and e) optical photographs of nano-CuO after standing for 30 days; (f) potential diagrams of nano-CuO at different times. Measurements were performed at a sample concentration of 0.6 mM, with the solution maintained at its natural pH under conditions of 25 ± 1 °C.

$$(\alpha h\nu)^{\frac{1}{n}} = A(h\nu - E_g) \quad (6)$$

where α represents the absorption coefficient of the incident photons, and $h\nu$ represents the energy of the incident photons. The value of the exponent n is closely related to the type of transition of the semiconductor material. Specifically, for semiconductor materials with a direct bandgap, the value of n is 1/2; while for semiconductor materials with an indirect bandgap, the value of n is 2.[44,45] A is a constant of proportionality. E_g represents the bandgap width of the material, and its value is determined by extrapolating the linear part of the curve to the x-axis. After calculation, the results are shown in Fig. 3(b). The bandgap value of the nano-copper oxide particles prepared in this study is 1.23 eV, which is consistent with those reported in the literature.[34,46–48]

3.2 Stability analysis of copper oxide nanodispersions

At room temperature, the nano-copper oxide powder (Sample No. 6) was redispersed in deionized water to obtain a nano-copper oxide dispersion. The dispersion stability of the nano-copper oxide particles in water was verified by observing the sedimentation situation of the dispersion and measuring the zeta potential of the dispersion. It should be noted that the products synthesized in the presence of CTAB and PVP exhibited sedimentation when left standing for 30 days, as detailed in ESI, Fig. S3† and 3(c–e) show that no phase separation was observed in the nano-copper oxide dispersion after the dispersion was left standing for 30 days. The zeta potential of the nano-copper oxide dispersion indicates that the surface charge values on the 1st, 7th, and 30th days of dispersion are −30.5 mV, −30.2 mV, and −30.3 mV, respectively, as shown in Fig. 3(f). These three values are very close to the specified threshold of ±30 mV, which demonstrates that the prepared nano-CuO has good redispersion stability and can be stored for a long time.

3.3 Copper oxide nanoparticles morphology and oxidation state analysis

The morphology of the synthesized product (Sample No. 6) was investigated by transmission electron microscopy (TEM). Fig. 4(a) shows that the as-prepared products exhibit an approximately spherical morphology. Lattice fringes of the product can be observed in Fig. 4(b), indicating a certain degree of crystallinity. Fig. 4(c) reveals that the average particle size of the product is 3–6 nm.

In order to study the oxidation states of the elements in the synthesized product, we further conducted X-ray photoelectron spectroscopy (XPS) tests on Sample No. 6, and recorded the full spectrum of the sample as well as the high-resolution scanning spectra of Cu, O and C. As shown in Fig. 5(a), the full spectrum indicates the presence of C, O, Cu and Na elements in the sample, with atomic percentages of 35.13%, 49.32%, 11.82%, and 3.73%, respectively. The possible reason for the presence of trace Na is the introduction of polymer sodium salt into the system during the preparation process. In the high-resolution spectrum of Cu 2p shown in Fig. 5(b), its energy level structure is mainly composed of Cu $2p_{3/2}$, the satellite peak, and Cu $2p_{1/2}$. Specifically, the peaks located at 933.88 eV and 953.9 eV correspond to Cu $2p_{3/2}$ and Cu $2p_{1/2}$, respectively. The difference in binding energy between the two is approximately 20 eV,[44] which is consistent with the spin splitting binding energy of the Cu 2p orbital.[49] In addition, the peaks appearing at 942.6 eV and 962.8 eV are attributed to the oscillatory satellite peaks of Cu $2p_{3/2}$ and Cu $2p_{1/2}$, respectively,[20] and are labeled as "Sat". This indicates the oxidation state of Cu^{2+} in the copper oxide nanoparticles and excludes the presence of copper ions in other states. Fig. 5(c) shows that the O 1s orbital consists of two peaks near 529.68 eV and 531.58 eV, which are attributed to O^{2-} in the copper oxide lattice and the chemically adsorbed oxygen on the surface, respectively.[44,49] Fig. 5(d) shows that the C 1s orbital consists of three peaks centered at approximately 284.78 eV, 286.78 eV, and 288.38 eV, which can be respectively assigned to C–C, C–O–C, and O–C=O bonds. These are attributed to adventitious carbon contamination or carbon sources derived from the protective agents. The adventitious carbon peak at 284.78 eV was used as a reference peak to calibrate the binding energy.[50]

3.4 Investigation on the photocatalytic capacity of copper oxide nanoparticles for methylene blue

3.4.1 Interaction of copper oxide nanoparticles with methylene blue. Currently, most of the literatures have reported the photocatalytic degradation mechanism of methylene blue (MB) by nano-copper oxide as a semiconductor,[7,51–53] while there are few literatures reporting the interaction between them. Therefore, we first studied the absorption spectra of MB in the range of 500–800 nm under different concentrations of nano-copper oxide without ultraviolet light illumination. The experimental results are shown in Fig. 6. Fig. 6(a) shows the experiment where 4 mL of MB with a concentration of 26.7 μM was taken, and then 1.5 mL of nano-copper oxide with concentrations of 0, 0.6, 1.3, 1.9, 2.5, 3.1, 3.8, 5.0, 6.3, and 7.5 mM were added to it respectively. As can be seen from the figure, the characteristic peaks of pure MB appear at 664 nm and 610 nm respectively. With the increase of the concentration of nano-copper oxide these two peaks gradually decrease until they almost disappear, and a new absorption peak appears at 583 nm, which increases with the increase of the concentration of nano-copper oxide. This indicates that a complex is formed between nano-copper oxide and MB. Fig. 6(b) shows the experiment in which 1.5 mL of nano-copper oxide with a concentration of 2.5 mM was taken and added respectively to 4 mL of MB with concentrations of 13.4, 21.4, 26.7, 32.1, 40.1, 48.1, 53.5, 58.8, 66.9, and 74.9 μM. As can be seen from the figure, when the concentration of the added MB is below 26.7 μM, the absorption peaks at 664 nm and 583 nm both exist. With the increase of the MB concentration, the absorption peak at 664 nm gradually strengthens. This result is basically consistent with that in Fig. 6(a).

In order to further explore the reason for the formation of a new complex between nano-copper oxide and MB, we respectively measured the zeta potentials of pure nano-copper

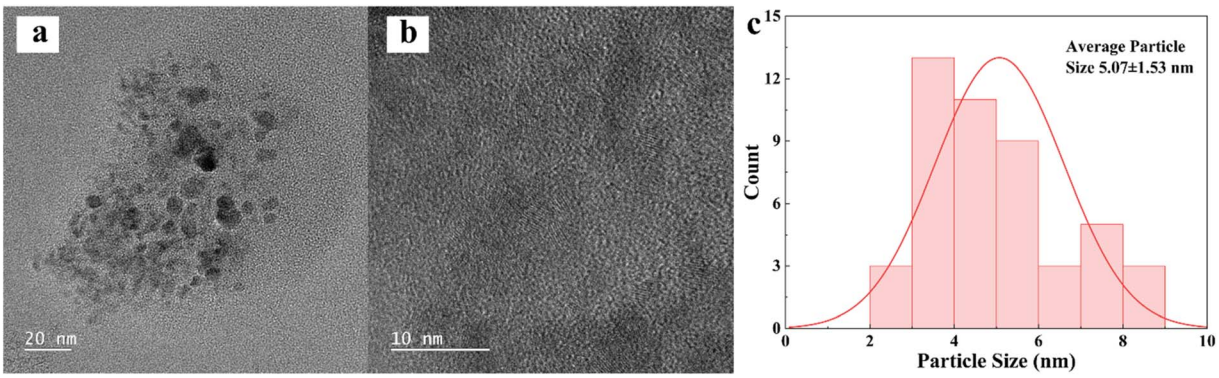

Fig. 4 (a) TEM image of Sample No. 6; (b) lattice fringe pattern of Sample No. 6; (c) particle size distribution histogram of Sample No. 6.

oxide, MB, and the system after complexation (2.5 mM nano-CuO, 26.7 μM MB). As shown in Fig. 6(c), it was found that the surface of nano-copper oxide a negative charge with a value of −30.5 mV, while the surface of MB carried a positive charge with a value of 17.1 mV. Compared with that of nano-copper oxide, the zeta potential value of the formed complex decreases, with a value of −17.2 mV. Thus, it can be speculated that the complex is formed due to the electrostatic interaction.

3.4.2 Investigation on the photocatalytic capacity of methylene blue by copper oxide nanoparticles. Different amounts of nano-copper oxide were taken and added respectively into a 40 mL MB solution with an initial concentration of 53.5 μM. A catalytic experiment was carried out under ultraviolet light with a wavelength of 365 nm. Samples were taken for testing every 20 minutes. The experimental results are shown in Fig. 7. Fig. 7(a–c) show the absorption spectra of MB measured

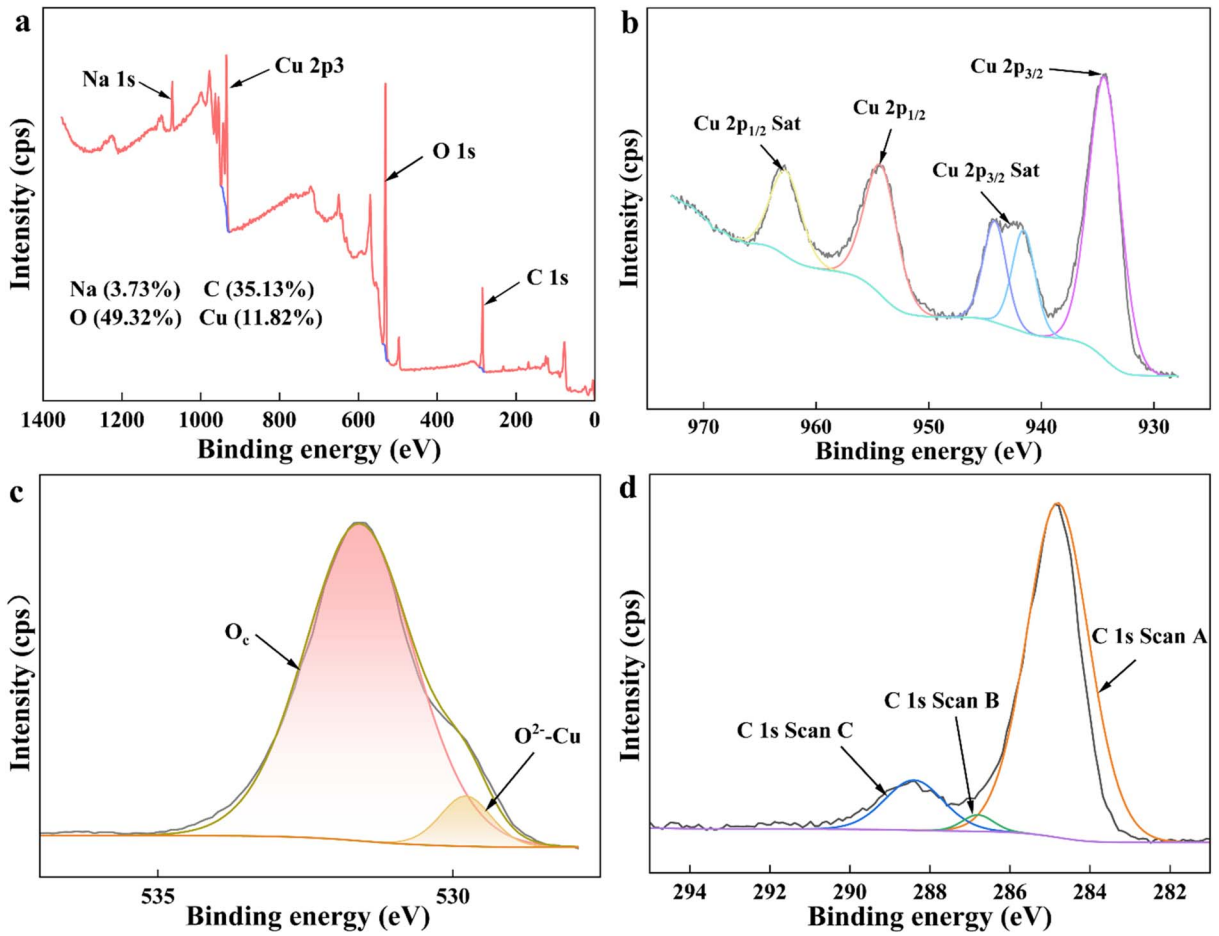

Fig. 5 (a) XPS full spectrum of nano-CuO; (b) peak-fitting diagram of Cu 2p for nano-CuO; (c) peak-fitting diagram of O 1s for nano-CuO; (d) peak-fitting diagram of C 1s for nano-CuO.

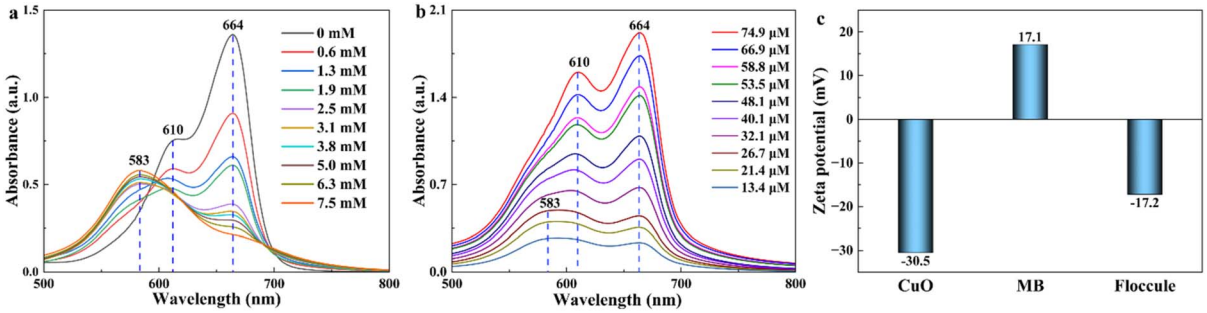

Fig. 6 In the mixed system of nano-CuO and MB: (a) absorption spectra of 26.7 μM MB with different amounts of nano-copper oxide; (b) absorption spectra of MB with different concentrations in the presence of 2.5 mM nano-CuO; (c) zeta potential diagrams of nano-CuO, MB and the complex formed after complexation.

during photocatalysis using 2.5 mM, 1.9 mM, and 1.3 mM of nano-copper oxide, respectively. It can be found that at 80 minutes, the concentrations of the systems decreased by only 9.9%, 8.8%, and 8.7%, respectively, indicating that the photocatalytic ability of nano-copper oxide is relatively weak. This result is distinct from the findings widely reported in current literature, which indicate that pure nano-copper oxide has a photocatalytic degradation effect of 50–90% on MB. This is quite astonishing, and this phenomenon warrants further in-depth investigation.

However, when only 0.6 mM of nano-copper oxide was added to the system, within the first 20 minutes of the reaction, as shown in Fig. 7(d), the concentration of the supernatant in the system decreased by 47.8%. Meanwhile, flocs were generated in the system, as depicted in Fig. 8(a and b). Such a phenomenon has not been reported in the relevant studies on the photocatalysis of methylene blue by nano-copper oxide. The system was then continuously placed under ultraviolet light and stirred for the catalytic experiment. At 80 minutes, compared with that at 20 minutes, the concentration of the supernatant decreased by only 6.5%, indicating that the photodegradation effect of the system was poor after 20 minutes.

Regarding the reasons for the appearance of flocs in the system and the significant decrease in concentration within the first 20 minutes, our analysis suggests that it is due to the relatively high concentration of MB in the system, which leads

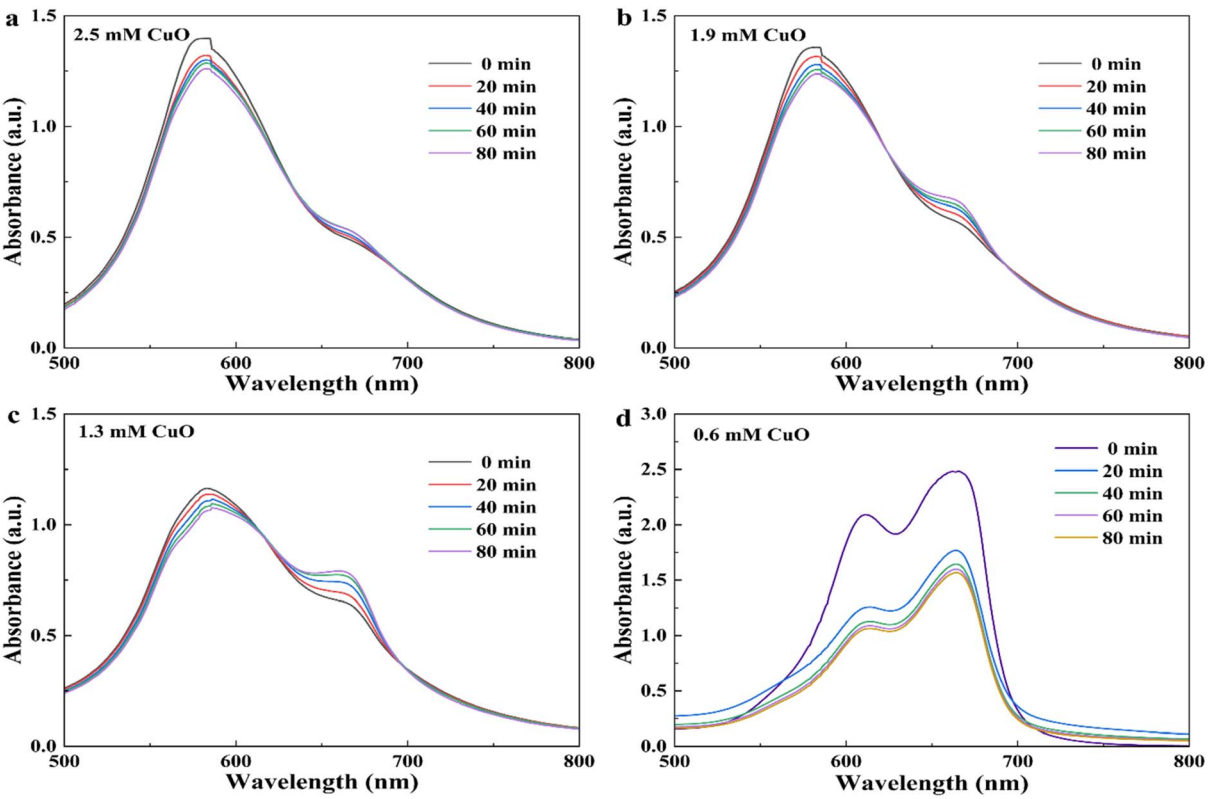

Fig. 7 Photodegradation spectra of MB with an initial concentration of 53.5 μM under different addition amounts of nano-CuO: (a) 2.5 mM; (b) 1.9 mM; (c) 1.3 mM; (d) 0.6 mM.

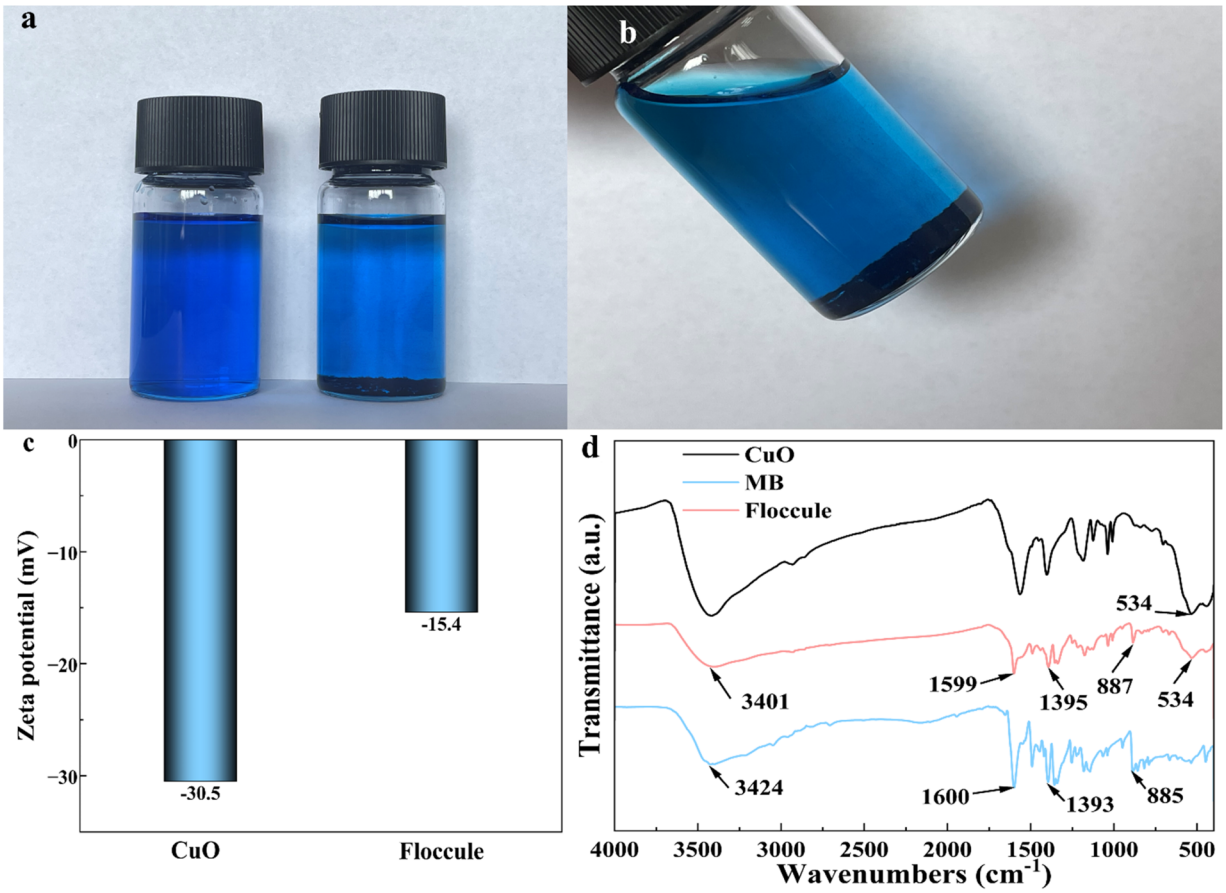

Fig. 8 (a and b) Optical photographs of the flocculent precipitates formed in the MB solution; (c) comparison of the zeta potentials of the nano-CuO dispersion liquid and the solution after the formation of the flocculates; (d) FT-IR spectra of CuO, MB and flocculates.

to a decrease in the charge of the nano-copper oxide colloidal dispersion, making the dispersion unstable. Further analysis was conducted through the zeta potential plot in Fig. 8(c). The results show that the charge of the supernatant after flocculation is −15.4 mV, and the absolute value of this charge has significantly decreased, which is consistent with our experimental speculation. In order to further explore the reason for the decrease in the concentration of MB during the flocculation process, the flocs were analyzed by Fourier transform infrared (FT-IR) spectroscopy, and the results are shown in Fig. 8(d). As can be seen from the FT-IR spectrum of the flocs, typical absorption peaks of pure MB appear at 1599 cm^{-1}, 1399 cm^{-1}, and 887 cm^{-1}, and the peak at 534 cm^{-1} belongs to the stretching vibration peak of the Cu–O bond. This result suggests that while MB was adsorbed by the nano-copper oxide during flocculation, it remained undegraded during photocatalysis. Calculated by formula (1), the adsorption capacity of nano-copper oxide was 217.4 mg g^{-1}. Thus, we conclude that the observed decrease in MB concentration was caused by adsorption and flocculation on nano-copper oxide, followed by solid–liquid separation. Therefore, we have good reason to tentatively speculate that the results of the catalysis of methylene blue by nanoscale copper oxide reported in the current literature may be due to adsorption separation rather than photocatalytic degradation.

3.5 Hydrogen peroxide enhanced photocatalytic capacity of nano-copper oxide

First, 0.5 mL of 30% (mass fraction) hydrogen peroxide (H_2O_2) was added to 40 mL of MB with an initial concentration of 53.5 μM as a blank control group to investigate its photocatalytic degradation effect on MB; the experimental results are shown in Fig. 9(a). The results indicate that under the sole action of H_2O_2, the MB concentration decreased by only 53.3% after 75 minutes. Subsequently, using 0.6 mM of nano-CuO as the catalyst, different amounts of 30% (mass fraction) H_2O_2 (0.5 and 1 mL) were added to the system to study the photocatalytic degradation efficiency of nano-CuO on MB in the presence of H_2O_2, as shown in Fig. 9(b and c). It can be clearly observed from the figures that the degradation rates of MB reached 87.4% and 99.6% at 75 minutes, respectively. At this point, the system with 1 mL of H_2O_2 became transparent without precipitates. This result indicates that nanoscale CuO still has good application prospects under the enhancement of H_2O_2. This is because, as an electron acceptor, H_2O_2 can effectively inhibit the recombination rate of electron–hole pairs on the surface of the catalyst to a certain extent. The reduction in electron–hole

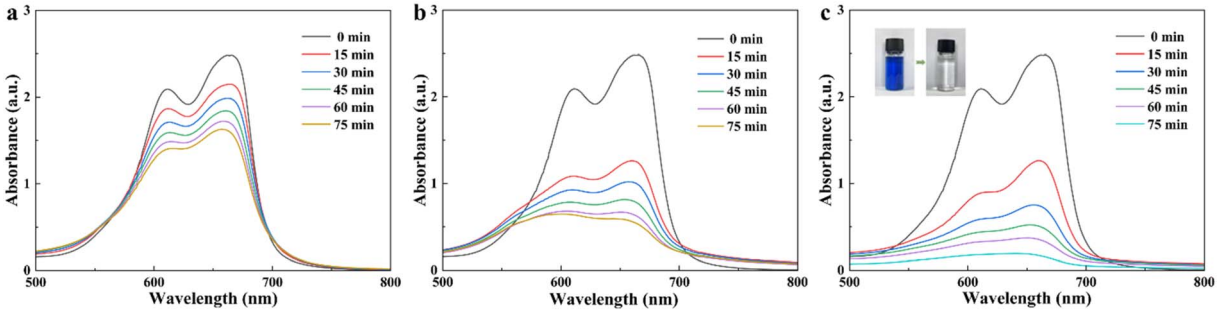

Fig. 9 Photodegradation diagram of MB (a) 0.5 mL H_2O_2 alone; (b) 0.5 mL H_2O_2 with 0.6 mM nano-CuO; (c) 1 mL H_2O_2 with 0.6 mM nano-CuO.

pair recombination promotes the generation of more hydroxyl radicals (·OH) and superoxide radicals ($\cdot O_2^-$), enhancing the oxidation capacity of the system and significantly improving the photocatalytic performance. During this process, the following main reactions occurred:

$$H_2O_2 + h\nu \rightarrow 2\cdot OH$$

$$H_2O_2 + \cdot O_2^- \rightarrow \cdot OH + OH^- + O_2$$

Subsequently, the first-order kinetic rate constants for the above reactions were calculated using eqn (7), as shown in ESI Fig S4,† yielding values of 0.008866 min^{-1}, 0.02508 min^{-1}, and 0.06391 min^{-1}, respectively.

$$\ln \frac{C_0}{C_t} = kt \quad (7)$$

where k is the rate constant in min^{-1}, C_0 is the dye concentration at $t = 0$, and C_t is the dye concentration at time t. From the rate constants, it can be seen that the system in Fig. 9(c) exhibits superior photocatalytic performance.

4 Conclusions

In conclusion, this work demonstrates a facile synthesis of redispersible CuO nanoparticles (92.18 nm) through ethyleneglycol-mediated complexation and poly(sodium 4-styrenesulfonate-*co*-maleate) stabilization. The colloidal system maintained superior stability (−30.5 to −30.3 mV Zeta potential) over 30 days without sedimentation. Charge-transfer complexation between nano-CuO and MB was mechanistically confirmed through dual evidence: (1) bathochromic spectral shift (664 → 583 nm) and (2) interfacial charge compensation effects. Photocatalytic ability tests revealed a special behavior: while higher catalyst loads (1.3–2.5 mM) showed marginal UV-driven degradation (8.7–9.9%), a distinctive adsorptive regime dominated at 0.6 mM dosage. FT-IR-verified adsorption achieved exceptional capacity (217.4 mg g^{-1}) through flocculation kinetics (54.3% supernatant reduction in 80 min). Strategic introduction of H_2O_2 enabled radical-mediated synergism, achieving complete MB degradation (99.6% of 53.5 μM solution within 75 min). These findings establish two critical advancements: (i) a promising methodology for engineering redispersible metal oxides, and (ii) a degradation process with adsorption as the primary focus and enhanced photocatalysis as the secondary focus provides new insights into the solution of organic water pollutants.

Data availability

Data are contained within the article.

Author contributions

Conceptualization, Z. C.; methodology, G. G.; validation, Q. W.; investigation, Q. W.; writing – original draft preparation, Q. W. and G. D.; writing – review and editing, Z. C. and G. D.; supervision, Z. C. All authors have read and agreed to the published version of the manuscript.

Conflicts of interest

The authors declare no conflicts of interest.

Acknowledgements

We gratefully acknowledge the financial support from the Fundamental Research Funds for the Central Universities (WHUT:2021III002).

References

1 J. Y. Lin, W. Y. Ye, M. Xie, D. H. Seo, J. Q. Luo, Y. H. Wan and B. van der Bruggen, *Nat. Rev. Earth Environ.*, 2023, **4**, 785–803.
2 S. W. Lee and H. C. Han, *Front. Neurosci.*, 2021, **15**, 663650.
3 C. Boillereau and S. Peulon, *J. Water Process Eng.*, 2023, **54**, 104024.
4 I. Khan, K. Saeed, I. Zekker, B. L. Zhang, A. H. Hendi, A. Ahmad, S. Ahmad, N. Zada, H. Ahmad, L. A. Shah, T. R. Shah and I. Khan, *Water*, 2022, **14**, 242.
5 M. Zou, C. Tan, X. L. Liu, Z. Q. Yuan, W. Q. Liu, L. Y. Zhang, X. Y. Yan, X. F. Zhao and H. Zhou, *J. Water Process Eng.*, 2024, **60**, 105200.
6 P. O. Oladoye, T. O. Ajiboye, E. O. Omotola and O. J. Oyewola, *Results Eng.*, 2022, **16**, 100678.

7 G. Sorekine, G. Anduwan, M. N. Waimbo, H. Osora, S. Velusamy, S. Kim, Y. S. Kim and J. Charles, *J. Mol. Struct.*, 2022, **1248**, 131487.
8 J. Di, J. Xiong, H. M. Li and Z. Liu, *Adv. Mater.*, 2018, **30**, 1704548.
9 G. Ebri and K. Hellgardt, *Chem. Eng. J.*, 2024, **486**, 150131.
10 A. Bashiri Rezaie, M. Montazer and M. Mahmoudi Rad, *J. Cleaner Prod.*, 2018, **204**, 425–436.
11 X. L. Hu, T. Y. Zhang, J. J. Chen, H. G. Gao and W. F. Cai, *Ceram. Int.*, 2016, **42**, 8505–8512.
12 J. F. Tan, M. H. Dun, L. Li, J. Y. Zhao, X. Li, Y. E. Hu, G. Huang, W. H. Tan and X. T. Huang, *Sens. Actuators, B*, 2017, **252**, 1–8.
13 G. Bhanjana, N. Dilbaghi, K. H. Kim and S. Kumar, *J. Mol. Liq.*, 2017, **244**, 506–511.
14 A. M. Soliman, M. Khalil and I. M. Ali, *J. Water Process Eng.*, 2021, **41**, 102086.
15 A. Ravikumar, V. Natraj, Y. Sivalingam, V. J. Surya, F. J. Zheng, H. J. Wang, Q. F. Du and N. Liu, *J. Mater. Chem. C*, 2022, **10**, 16492–16505.
16 S. Ihsan, H. Munir, Z. Meng, M. Tayyab, N. Zeeshan, A. Rehman, S. Nadeem and M. Irfan, *Int. J. Biol. Macromol.*, 2024, **268**, 131600.
17 M. J. Hong, M. S. Kim, S. B. Lee, S. K. Kim, Y. J. Kim and G. J. Lee, *ACS Appl. Mater. Interfaces*, 2024, **16**, 58556–58565.
18 S. Banerjee, S. Sarkar, S. Sarkar and A. K. Patra, *Inorg. Chem. Commun.*, 2024, **160**, 111925.
19 X. Li, X. Zhao, J. Lv, X. Jia, S. Zhou, Y. Huang, F. Chang, H. Zhang and G. Hu, *J. Mater. Sci. Technol.*, 2023, **137**, 104–111.
20 B. K. Singh, A. Shaikh, R. O. Dusane and S. Parida, *J. Energy Storage*, 2020, **31**, 101631.
21 N. K. Farhana, Z. L. Goh, N. M. Saidi, F. S. Omar, S. Bashir, S. Ramesh and K. Ramesh, *Mater. Today Commun.*, 2024, **38**, 107966.
22 R. Ahmad, M. A. Yewale, M. Khan, U. T. Nakate, A. Ahmad, M. B. Alshammari, K. D. Bhalerao, K. S. Bhat and B.-I. Lee, *Sens. Actuators, B*, 2024, **415**, 135979.
23 P. Raizada, A. Sudhaik, S. Patial, V. Hasija, A. A. P. Khan, P. Singh, S. Gautam, M. Kaur and V. H. Nguyen, *Arabian J. Chem.*, 2020, **13**, 8424–8457.
24 W. M. Rangel, R. Santa and H. G. Riella, *J. Mater. Res. Technol.*, 2020, **9**, 994–1004.
25 X. T. Mai, T. M. Duong, D. N. Nguyen, T. H. To, H. H. Luc, P. D. Tran and L. T. Le, *Energy Technol.*, 2025, **13**, 2401486.
26 H. Liu, S. Z. Wang, R. S. Zhuo, Y. W. Duan, J. L. Wang, Y. H. Li and J. Q. Yang, *Powder Technol.*, 2024, **444**, 119803.
27 A. Khan, Z. Tariq and M. H. Malik, *Mater. Lett.*, 2022, **324**, 132625.
28 K. H. Kim, H. Kawai, Y. Abe, M. Kawamura and T. Kiba, *J. Electron. Mater.*, 2018, **47**, 7296–7300.
29 M. Iqbal, A. A. Thebo, A. H. Shah, A. Lqbal, K. H. Thebo, S. Phulpoto and M. A. Mohsin, *Inorg. Chem. Commun.*, 2017, **76**, 71–76.
30 A. Muthuvel, M. Jothibas and C. Manoharan, *Nanotechnol. Environ. Eng.*, 2020, **5**, 14.
31 K. K. Anna, N. K. R. Bogireddy and R. Ramírez-Bon, *Nanotechnology*, 2021, **32**, 105707.
32 N. Benhadria, M. Hachemaoui, F. Zaoui, A. Mokhtar, S. Boukreris, T. Attar, L. Belarbi and B. Boukoussa, *J. Cluster Sci.*, 2021, **33**, 249–260.
33 S. Rakshit, K. G. Mondal, P. C. Jana, T. Kamilya and S. Saha, *J. Mater. Sci.: Mater. Electron.*, 2023, **34**, 2141.
34 N. F. A. Neto, P. M. Oliveira, R. M. Nascimento, C. A. Paskocimas, M. R. D. Bomio and F. V. Motta, *Ceram. Int.*, 2019, **45**, 651–658.
35 M. Shaheen, N. H. Kalwar, A. Intisar, Z. Batool, S. Rasheed and R. Kousar, *Opt. Mater.*, 2021, **122**, 111688.
36 A. S. Adeleye, S. Pokhrel, L. Mädler and A. A. Keller, *Water Res.*, 2018, **132**, 12–22.
37 F. Pellegrino, L. Pellutiè, F. Sordello, C. Minero, E. Ortel, V. D. Hodoroaba and V. Maurino, *Appl. Catal., B*, 2017, **216**, 80–87.
38 S. S. G. Srinivasan, B. Govardhanan, P. Aabel, M. Ashok and M. C. S. Kumar, *Sol. Energy*, 2019, **187**, 368–378.
39 J. Chen, M. D. Tu, M. Y. Xu, D. P. Gong, X. Li and C. C. Zhang, *Nanomaterials*, 2024, **14**, 852.
40 J. Wang, X. Yang, J. J. Klemes, K. Tian, T. Ma and B. Sunden, *Renewable Sustainable Energy Rev.*, 2023, **188**, 113854.
41 T. M. D. Dang, T. T. T. Le, E. Fribourg-Blanc and M. C. Dang, *Adv. Nat. Sci.: Nanosci. Nanotechnol.*, 2011, **2**, 015009.
42 M. Bin Mobarak, F. Chowdhury and S. Ahmed, *RSC Adv.*, 2024, **14**, 39874–39889.
43 R. C. Kasana, N. R. Panwar, U. Burman and P. Kumar, *Inorg. Nano-Met. Chem.*, 2022, **54**, 120–125.
44 C. Gherasim, P. Pascariu, M. Asandulesa, M. Dobromir, F. Doroftei, N. Fifere, A. Dascalu and A. Airinei, *Ceram. Int.*, 2022, **48**, 25556–25568.
45 N. Fifere, A. Airinei, D. Timpu, A. Rotaru, L. Sacarescu and L. Ursu, *J. Alloys Compd.*, 2018, **757**, 60–69.
46 L. H. Xu, Y. Zhou, Z. J. Wu, G. G. Zheng, J. J. He and Y. J. Zhou, *J. Phys. Chem. Solids*, 2017, **106**, 29–36.
47 Y. Chen, L. Zhang, H. Zhang, K. Zhong, G. Zhao, G. Chen, Y. Lin, S. Chen and Z. Huang, *Ceram. Int.*, 2018, **44**, 1134–1141.
48 H. Absike, M. Hajji, H. Labrim, A. Abbassi and H. Ez-Zahraouy, *Superlattices Microstruct.*, 2019, **127**, 128–138.
49 J. Sackey, A. C. Nwanya, A. K. H. Bashir, N. Matinise, J. B. Ngilirabanga, A. E. Ameh, E. Coetsee and M. Maaza, *Mater. Chem. Phys.*, 2020, **244**, 122714.
50 T. Saha, M. Bin Mobarak, M. N. Uddin, M. S. Quddus, M. R. Naim and N. S. Pinky, *Mater. Chem. Phys.*, 2023, **305**, 127979.
51 S. Arif, I. Javaid, Z. Israr, S. S. A. Gillani and M. S. Anwar, *Mater. Sci. Eng., B*, 2024, **310**, 117749.
52 S. Jabeen, V. U. Siddiqui, S. Bala, N. Mishra, A. Mishra, R. Lawrence, P. Bansal, A. R. Khan and T. Khan, *ACS Omega*, 2024, **9**, 30190–30204.
53 S. Jabeen, V. U. Siddiqui, S. Rastogi, S. Srivastava, S. Bala, N. Ahmad and T. Khan, *Mater. Today Chem.*, 2023, **33**, 101712.